

**Neutron and photon production from thick targets
bombarded by 30-MeV p, 33-MeV d, 65-MeV ^3He , and 65-MeV α ions:
Phenomenological analysis of experimental neutron energy spectra**

T. Nakamura and Y. Uwamino

Institute for Nuclear Study, University of Tokyo, Midori-cho 3-2-1, Tanashi, Tokyo, Japan

(Received 8 November 1983)

The measured energy spectra, reported in the preceding paper, of neutrons produced from thick carbon, copper, and lead targets exposed to 30-MeV protons, 33-MeV deuterons, 65-MeV ^3He , and 65-MeV alpha particles were analyzed with the phenomenological hybrid model of equilibrium and preequilibrium emissions, together with the Serber model for deuteron stripping. Both spectral components of equilibrium and preequilibrium were well fitted to two Maxwellian-type functions having different nuclear temperatures. The former temperature values were only a function of the excited energy of the compound nucleus per nucleon, independently of the neutron emission angle, while on the other hand, the latter temperature values were dependent on the emission angle and the total energy delivered into the compound nucleus by the projectile. For deuteron, ^3He , and alpha projectiles, a broad bump was seen in the forward spectrum which corresponds to the direct knockout and the deuteron and ^3He breakup processes. The deuteron breakup process calculated by the Serber model showed rather good agreement with the measured spectrum.

I. INTRODUCTION

The inclusive cross section measurements of single-particle, usually proton or neutron, emission from various thin targets have been performed for light and heavy projectiles of energies lower than about 100 MeV/nucleon. The measured neutron spectra emitted from proton,¹⁻⁴ ^3He ,⁵ alpha,⁶ and heavy ion⁷ reactions were analyzed by the hybrid model of evaporation (equilibrium) in the lower energy region and preequilibrium in the higher energy region. They were well represented by the combination of evaporation neutrons from a compound nucleus having a nuclear temperature of 1–2 MeV which is independent of the neutron emission angle, and preequilibrium components from a precompound nucleus having a nuclear temperature of 4–5 MeV or more which is dependent on the emission angle.

The neutron spectra from thick targets have also been published for various projectile-target combinations. The works were analyzed with the Monte Carlo calculation based on the intranuclear-cascade evaporation model for projectile energies higher than 100 MeV/nucleon,⁸⁻¹² except for only one work of ours.¹³ This calculational model is valid for a projectile energy of 50 MeV/nucleon as described in the preceding paper, and moreover does not give the direct connection between the reaction mechanism and the resultant neutron spectrum, due to its statistical simulation. There has been no work published on the analysis of the thick-target neutron spectrum connecting to the mechanism to produce neutrons from nucleon-nucleus and nucleus-nucleus collisions, except for the neutron spectrum analysis on the basis of the Serber model¹⁴ for deuteron stripping.^{15,16}

Here in this study, we first aimed to analyze our experimental thick-target neutron spectra from 30-MeV proton,¹³ 33-MeV deuteron, 65-MeV ^3He , and 65-MeV alpha

projectiles given in the preceding paper, by using the phenomenological hybrid model of equilibrium and preequilibrium emissions as in the thin-target neutron spectrum analysis, together with the Serber model for deuteron stripping.

II. EVALUATION OF EVAPORATION NEUTRON SPECTRA

The evaporation cross section in the center of mass (c.m.) system is given by

$$\frac{d^2\sigma}{d\epsilon d\Omega} = \sigma_{\text{nonel}} \frac{K}{4\pi} \frac{\epsilon}{T^2} \exp\left[-\frac{\epsilon}{T}\right], \quad (1)$$

[in (cm²/MeV sr)] since the evaporated neutrons are emitted isotropically in the c.m. system, where ϵ is the neutron energy in the c.m. system, in MeV; Ω is the solid angle in the c.m. system; σ_{nonel} is the nonelastic cross section; K is the total number of evaporated neutrons per nonelastic collision; and T is the nuclear temperature, in MeV.

The emission angles in the c.m. system and the laboratory (L) system are assigned to be Θ and θ , respectively, and the evaporation cross section in the L system is obtained from Eq. (1) as

$$\frac{d^2\sigma}{dE d\theta} = \sigma_{\text{nonel}} \frac{K}{2} \frac{\sqrt{E\epsilon}}{T^2} \exp\left[-\frac{\epsilon}{T}\right] \sin\theta |J|, \quad (2)$$

[in (cm²/MeV sr)] where E is the neutron energy in the L system, in MeV;

$$|J| = \frac{\partial(\epsilon, \Theta)}{\partial(E, \theta)} = 1.$$

The relation between E and ϵ is obvious,

TABLE I. Parameters A_1 and A_2 in Eq. (6) of the total evaporation neutron yield by proton bombardment.

Target	A_1	A_2
C	0.624	0.202
Cu	1.26	0.730
Pb	4.95	2.24

$$\epsilon = E + E_c - 2\sqrt{EE_c}\cos\theta, \quad (3)$$

$$E_c = \frac{M_i M_n}{(M_i + M_t)^2} E_i,$$

where M_i , M_n , and M_t are atomic masses of the projectile, neutron, and target nucleus, respectively, and E_i is the projectile kinetic energy in the L system.

The evaporation neutron spectrum of the thick target observed in the L system, $\Phi(E, \theta)$, is given by

$$\Phi(E, \theta) = \int_{E_{th}}^{E_0} N \sigma_{\text{nonel}}(E_i) \frac{K}{2} \frac{\sqrt{E}\epsilon}{T^2} \times \exp\left[-\frac{\epsilon}{T}\right] \left[\frac{dE_i}{dx}\right]^{-1} dE_i, \quad (4)$$

[in (MeV sr projectile) $^{-1}$], where E_0 is the initial kinetic energy of the projectile, in MeV; E_{th} is the threshold energy of the neutron produced reaction, in MeV; N is the atomic density of the target, in atoms/cm 3 ; E_i is the projectile kinetic energy in the target, in MeV; and dE_i/dx is the stopping power of the projectile, in MeV/cm.

The nonelastic cross section, $\sigma_{\text{nonel}}(E_i)$, for the proton incidence was given from its analytical representation based on the intranuclear-cascade evaporation Monte Carlo calculation¹⁷ as

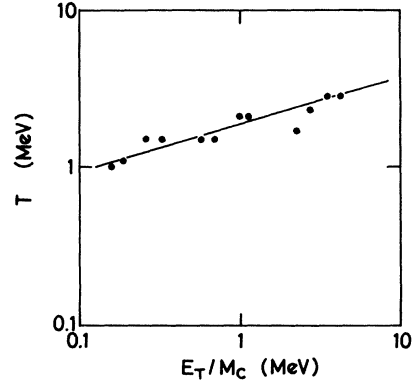


FIG. 1. Dependence of the nuclear temperature T of the compound nucleus in an equilibrium state on its excited energy per nucleon, E_T/M_C , where E_T and M_C are the excited energy and the atomic mass of the compound nucleus, respectively.

$$\sigma_{\text{nonel}}(E_i) = \frac{1}{400} \exp\left\{\sum_{j=0}^{\nu} a_j \left[\frac{E_i}{400}\right]^j\right\} \times 10^{-27}, \quad (5)$$

(in cm 2) where a_j is the constant given in Ref. 17. There are no data of $\sigma_{\text{nonel}}(E_i)$ for projectiles other than the proton, so they were replaced by the values of $\sigma_{\text{nonel}}(E_i)$ for the proton. The total number of evaporated neutrons, K , was also estimated from the following analytical fit to the results given in Ref. 17,

$$K = -A_1 + A_2 \ln E_i \quad (6)$$

(neutrons/nonelastic collision), and the parameters A_1 and A_2 are shown in Table I. Since there are also no data of K for projectiles other than the proton, the values of K for

TABLE II. Q value and excited energy per nucleon of the compound nucleus; ratio of calculated and measured total evaporation neutrons, $K_{\text{exp}}/K_{\text{cal}}$; and nuclear temperature T for the equilibrium state and T' for the preequilibrium state, for each projectile-target combination.

Projectile	Energy		Compound nucleus	Q (MeV)	Excited energy per nucleon ($E_0 + Q$)/ M_c (MeV)		$\frac{K_{\text{exp}}}{K_{\text{cal}}}$	Equilibrium T (MeV)	Nuclear temperature Preequilibrium, T' (MeV)				
	E_0 (MeV)	Target			$E_0 + Q$ (MeV)	$(E_0 + Q)/M_c$ (MeV)			0°	15°	45°	75°	135°
p	30	^{12}C	^{13}N	1.94	2.28	2.9	1.7						
		^{63}Cu	^{64}Zn	7.71	0.58	0.96	1.5	4.7	4.6	3.9	3.6	2.6	
		^{208}Pb	^{209}Bi	3.71	0.16	0.67	1.0	4.4	4.3	4.1	3.8	3.3	
d	33	^{12}C	^{14}N	10.27	2.75	11.4	2.3	9.3	7.0	5.0	3.9		
		^{63}Cu	^{65}Zn	13.46	0.70	1.32	1.5	6.9	5.9	4.3	3.3	2.7	
		^{208}Pb	^{210}Bi	6.19	0.19	0.93	1.1	5.0	4.9	4.3	3.3	3.3	
^3He	65	^{12}C	^{15}O	12.08	4.27	5.2	2.8	11.2	9.8	8.3	6.3	4.2	
		^{63}Cu	^{66}Ga	13.07	1.13	1.11	2.1	9.8	9.0	6.9			
		^{208}Pb	^{211}Po	5.63	0.33	0.79	1.5	10.2	8.2	5.8			
α	65	^{12}C	^{16}O	7.16	3.49	2.6	2.8	7.4	5.5	4.6	4.6	3.0	
		^{63}Cu	^{67}Ga	3.72	0.97	1.06	2.1	7.3	6.8	6.7	5.9	3.5	
		^{208}Pb	^{212}Po	-8.94	0.26	0.40	1.5	6.2	5.4	5.0	4.7	3.6	

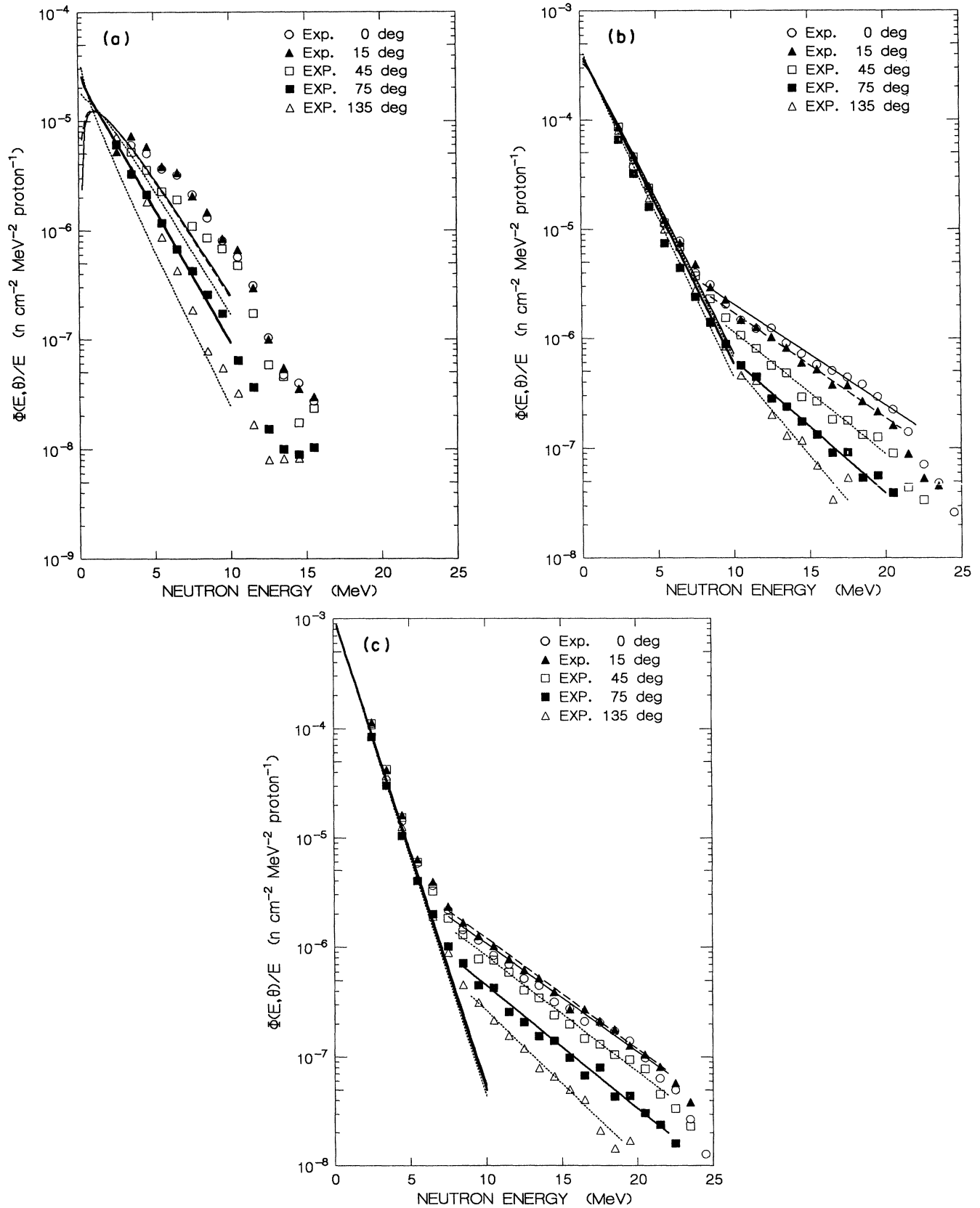


FIG. 2. Analytical fitting of the measured neutron spectra divided by the neutron energy E of $\Phi(E, \theta)/E$ at θ emission angle by 30-MeV proton bombardment to two Maxwellian-type spectra having nuclear temperatures T for evaporation neutrons and $T'(\theta)$ for preequilibrium emission. The experimental errors are omitted in all graphs of this paper just for simplicity, since they are already shown in the preceding paper. (a) Carbon target. (b) Copper target. (c) Lead target.

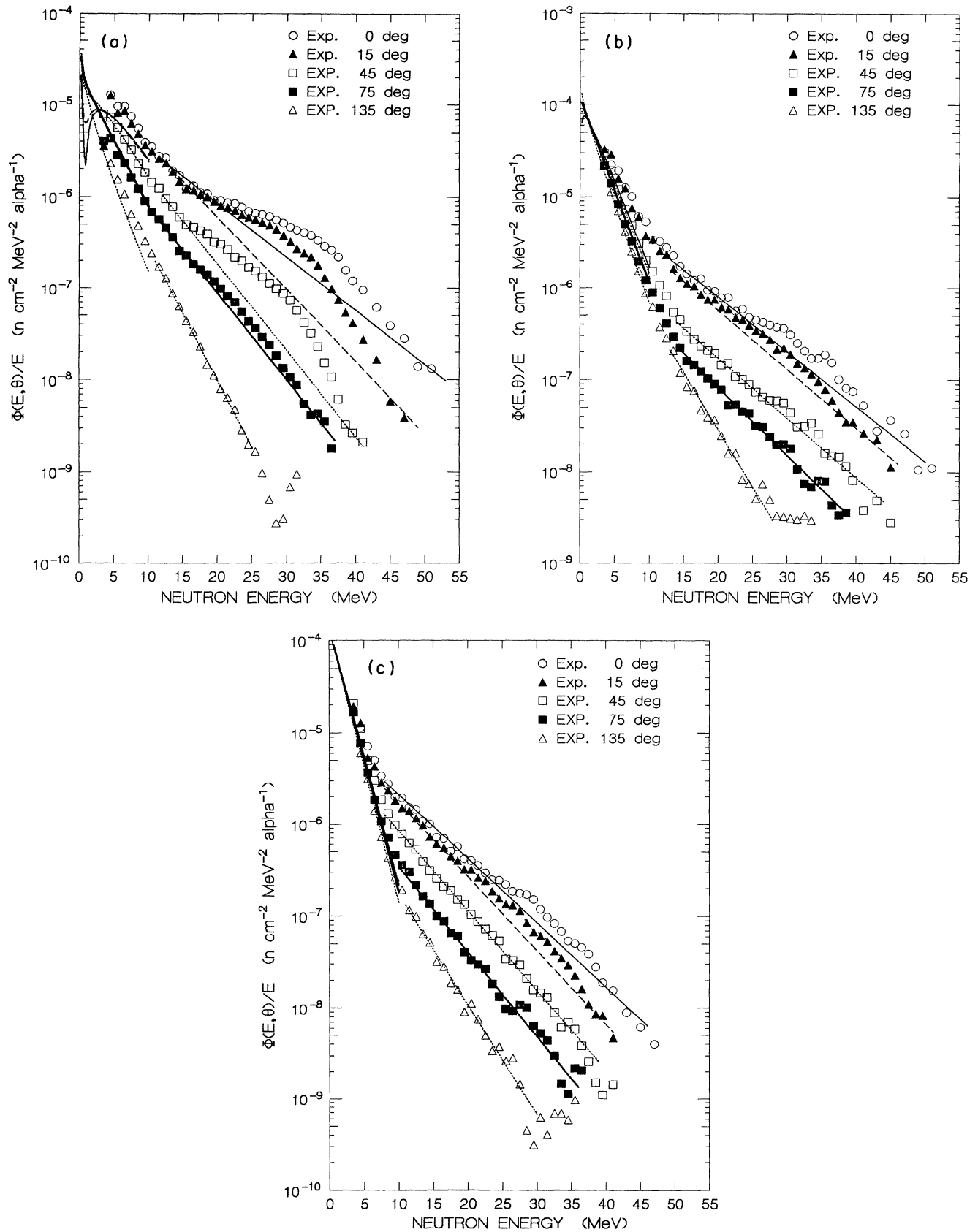


FIG. 3. Analytical fitting of the measured neutron spectra $\Phi(E, \theta)/E$ by 65-MeV alpha ion bombardment to two Maxwellian-type spectra having nuclear temperatures T and $T'(\theta)$ as in Fig. 2. (a) Carbon target. (b) Copper target. (c) Lead target.

the proton were used instead, considering that the evaporation process is ruled only by the excited energy of the compound nucleus, independently of the projectile type. As a result, the projectile energy E_i in Eq. (6) was replaced by E'_i given as

$$E'_i = E_i + \Delta Q, \quad (7)$$

$$\Delta Q = [(M_i + M_i)c^2 - M_C c^2] - [(M_i + M_p)c^2 - M_C c^2],$$

where M_i and M_C are the atomic masses of the projectile and compound nucleus for incident particles other than the proton, and M_p and M_C are the atomic masses of the proton and compound nucleus, respectively, for the proton incidence. The values of dE_i/dx were cited from Ref. 18 and E_{th} was fixed to be the energy at which $K=0$ in Eq. (6), but E_{th} was set to be equal to the Coulomb barrier when the former energy became less than the Coulomb barrier.

By using these quantities, $\Phi(E, \theta)$ was calculated by numerical integration of Eq. (4) for various values of the nuclear temperature T . The values of T best fitted to the measured neutron spectra are shown in Table II for each projectile and target combination. As seen in Table II, the T value is dependent on the total energy E_T delivered into the target nucleus by the projectile, which is given by

$$E_T = E_0 + Q, \quad (8)$$

and the Q values for forming the compound nucleus are also shown in Table II. As the evaporation neutrons are emitted from an equilibrium state of the compound nucleus whose energy is equidistributed among nucleons, the nuclear temperature must be a function of the excited energy of the compound nucleus per nucleon, E_T/M_C , as is shown in Fig. 1. From Fig. 1, the relationship between T and E_T/M_C can be derived approximately as

$$T = 1.85(E_T/M_C)^{0.3}, \quad (9)$$

in the projectile energy region from 0.1 to 10 MeV/nucleon, almost independently of the types of projectile and target nuclei.

The thick-target neutron spectra calculated by using the T values in Table II are compared with the measured neutron spectra for proton and alpha projectiles in Figs. 2 and 3, respectively, as examples. As ϵ approaches E , $\Phi(E, \theta)$ becomes a function of $E \exp(-E/T)$, and this comparison was done in the form of $\Phi(E, \theta)/E$. When the target atomic mass M_i is small like carbon, E is strongly dependent on the emission angle, θ , in the L system, as seen from Eq. (3), so the calculated $\Phi(E, \theta)$ value varied with θ for the carbon target, but with an increase in the target atomic mass from copper towards lead, the change of $\Phi(E, \theta)$ with θ became considerably smaller, as seen in Figs. 2 and 3. The comparison of $\Phi(E, \theta)$ calculated and measured is done in relative values in Figs. 2 and 3, and the normalization constants are shown in Table II. These normalization constants correspond to the ratio of measured and calculated total number of evaporated neutrons, K_{exp}/K_{cal} , and the values of K_{exp}/K_{cal} are close to 1 for the copper target, and for the carbon target the calculated values of the evaporation neutron yields are 2 to 3 times

smaller than the measured results, except for the deuteron and ^3He projectiles which cause a dominant stripping reaction. This underestimation comes from the fact that the K value obtained by Eq. (6) is based on the intranuclear-cascade evaporation calculation given in Ref. 17, which is not so good for a lighter target nucleus and for a projectile of energy lower than about 50 MeV/nucleon. In the several MeV region, the calculated evaporation neutron spectra well reproduce the measured results in their spectral shapes and their relative intensities among emission angles of 0 to 135 deg, except for the forward neutron emission from the carbon target exposed to deuteron and ^3He particles, where stripping reactions will still be dominant in this low energy region.

III. PHENOMENOLOGICAL HYBRID ANALYSIS OF NEUTRON ENERGY SPECTRA

The neutron spectra, $\Phi(E, \theta)/E$, exemplified in Figs. 2 and 3, are clearly divided into two components having different slopes. The low energy component having the steeper slope corresponds to the evaporation process as described in the preceding section, and the high energy component having the slower slope corresponds to the preequilibrium emission. The transition energies from equilibrium emission to preequilibrium emission in the neutron spectra are about 5–7 MeV at small emission angles of 0 to 15 deg and about 8–10 MeV at large emission angles of 75 to 135 deg. The neutron spectra emitted from the precompound nucleus may also be expressed in a Maxwellian-type spectrum above that transition energy, and as a result the plot of $\Phi(E, \theta)/E$ in a semilogarithmic scale gives an exponential function of $\exp(-E/T')$, as clearly seen in Figs. 2 and 3. Differently from the evaporation process, the nuclear temperature T' of a precompound nucleus in a preequilibrium state is dependent on the neutron emission angle θ and is, of course, higher than the nuclear temperature T of a compound nucleus in an equilibrium state, since the neutron emission from the hotter preequilibrium state occurs in a more forward direction. The values of T' obtained from the exponential fitting to the measured results of $\Phi(E, \theta)/E$ in Figs. 2 and 3 are also listed in Table II as a function of θ for all projectiles and targets, except for the proton incidence on the carbon target, where very few neutrons of energy above 12 MeV could be observed, because the Q value of the most probable neutron production reaction, $^{12}\text{C}(p, n)$, is -18.14 MeV. The T' values certainly decrease with θ and are about 3–5 MeV for 30-MeV protons, 3–7 MeV for 33-MeV deuterons, 4–10 MeV for 65-MeV ^3He , and 3–7 MeV for 65-MeV alpha particles. Generally speaking, T' is dependent on the total energy delivered into the compound nucleus from the projectile, E_T , in Eq. (8), rather than the total energy per nucleon, E_T/M_C , in contrast to T . This tendency may be reduced to the idea that the total energy delivered, E_T , will not be equally distributed among all of the nucleons in a preequilibrium state.

For the alpha projectile shown in Fig. 3, the $\Phi(E, \theta)/E$ spectra show a broad bump from their exponential form in the energy region from about 15 to about 45 MeV for all targets. The magnitude of the bump and its most

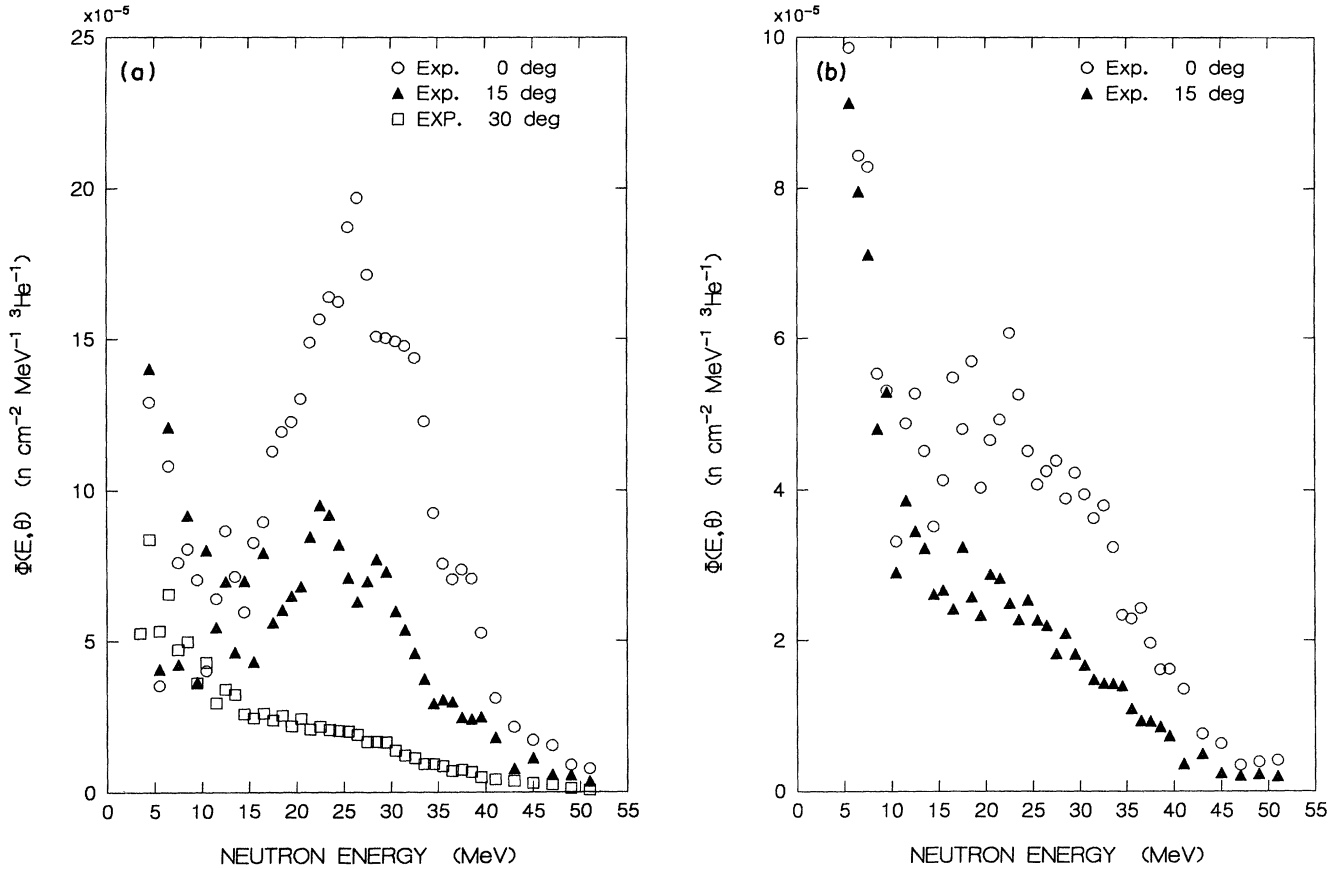


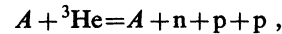
FIG. 4. Measured neutron spectra $\Phi(E,\theta)$ in the forward direction by 65-MeV ${}^3\text{He}$ bombardment. A broad peak corresponds to the ${}^3\text{He}$ breakup process. (a) Carbon target. (b) Copper target.

probable energy decrease with increasing emission angle and target atomic number. This shows that the reaction process which leads to the bump spectra is the direct knockout reaction.

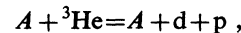
IV. ANALYSIS OF NEUTRON SPECTRA FROM PROJECTILE BREAKUP

As already shown in Figs. 3 and 4 of the preceding paper, the neutron spectra emitted in the forward direction have a broad remarkable peak above 10 MeV on the continuum spectra for the deuteron and ${}^3\text{He}$ incidences. The magnitude of this peak is larger for the deuteron than for ${}^3\text{He}$, and both of them are very much greater than the broad bump for the alpha projectile described before. The neutrons in this peak area are produced from the breakup reaction of deuteron and ${}^3\text{He}$ nuclei, (d,np) and (${}^3\text{He}$,n2p) reactions. Figure 4 shows the neutron spectra emitted in the forward direction from carbon and copper targets by a 65-MeV ${}^3\text{He}$ projectile. The most probable energies of these peaked neutron spectra are about 26 MeV for the carbon target and about 22 MeV for the copper target, which are close to $\frac{1}{3}$ of the incident kinetic energy of the ${}^3\text{He}$ projectile. The peak area decreases rapidly with emission angle, and at 30 deg for carbon, at 15 deg for copper, and even at 0 deg for lead, no peak can be seen on the continuum spectra due to the precompound neutron emission described before. The shape of the neutron spectra of the

carbon target resembles well the shape of the proton spectra of the thin ${}^{90}\text{Zr}$ target bombarded by 70-MeV ${}^3\text{He}$,¹⁹ in spite of different conditions. The neutron energy spectrum based on the direct breakup process,



cannot be calculated by a simple model, although the deuteron spectrum based on the direct breakup process,



has been calculated by the Serber model¹⁴ in Ref. 19.

The neutron energy spectrum based on the deuteron breakup process was analyzed on the basis of the Serber model, an elegantly simple semiclassical theory for deuteron stripping. The stripping neutron spectrum at 0 deg for deuterons of energy E_0 incident on a thick target can be written in general as

$$\Phi(E,0) = N \int_0^{E_0} \left[\frac{d^2\theta}{dE d\Omega} \right]_{\theta=0^\circ} \left[\frac{dE_d}{dx} \right]^{-1} dE_d, \quad (10)$$

where E_d is the deuteron kinetic energy in a thick target. The kinetic energy of the deuteron when it reaches the nucleus is reduced by the energy of the Coulomb barrier. The barrier energy E_C is expressed by

$$E_C = \frac{Z_A e^2}{R_A 1.6 \times 10^{-6}} \quad (11)$$

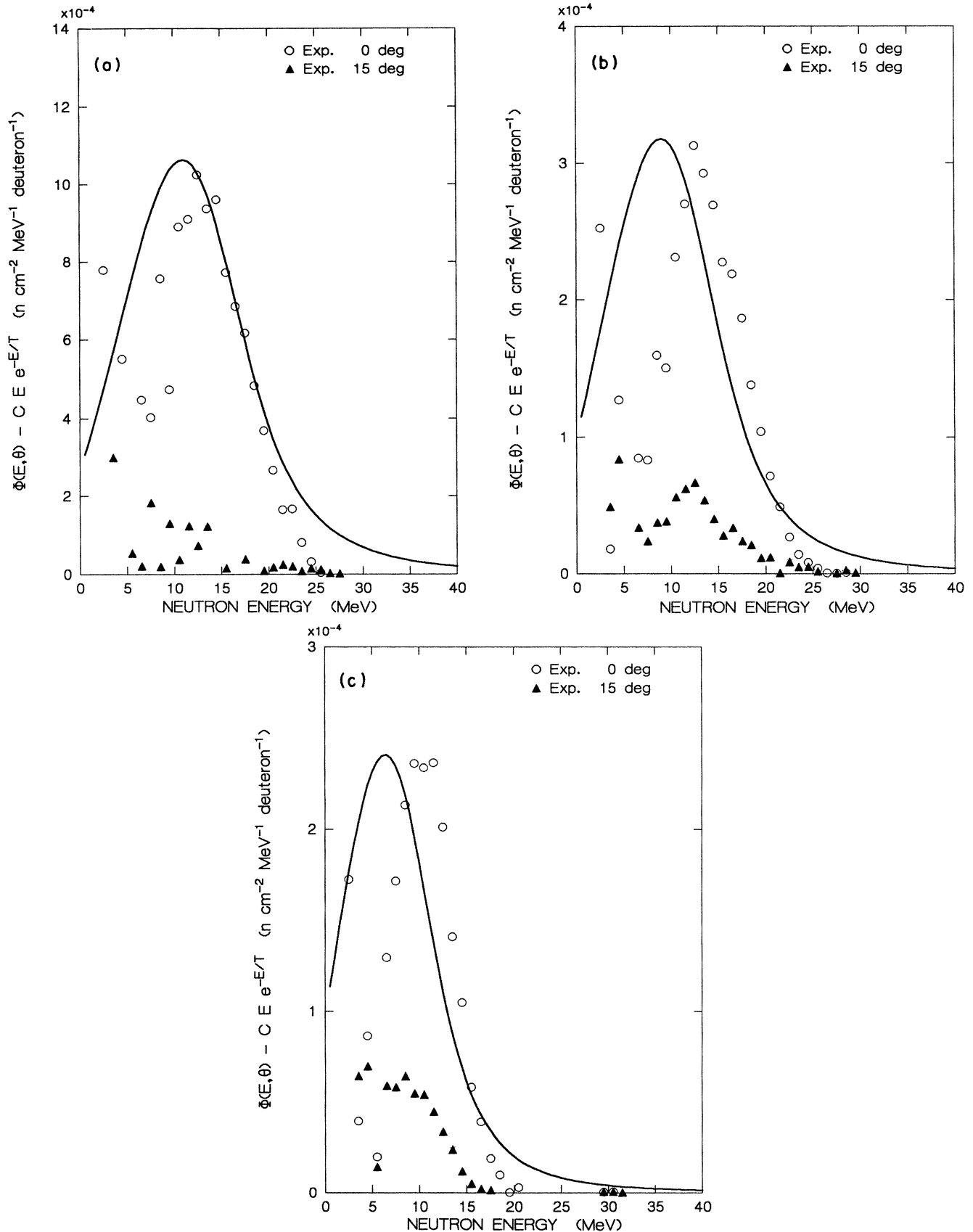


FIG. 5. Comparison of the measured neutron spectra minus the preequilibrium continuum spectra, $\Phi(E, \theta) - C E e^{-E/T(\theta)}$, by 33-MeV deuteron bombardment with those calculated by the Serber model for the deuteron stripping reaction. (a) Carbon target. (b) Copper target. (c) Lead target.

(in MeV), where Z_A is the atomic number of target nucleus, and R_A is the radius of target nucleus, $1.4 \times 10^{-13} \times M_t^{1/3}$ cm. The double differential cross section of deuteron stripping, $d^2\sigma/dE d\Omega$, is approximated by the Serber differential cross section, $d\sigma/dE$, in the forward direction and the full-width at half-maximum neutron flux of the stripping neutron angular distribution, $\Delta\theta_{1/2}$, as follows,

$$\left(\frac{d^2\sigma}{dE d\Omega} \right)_{\theta=0^\circ} = \frac{d}{d\Omega} \left(\frac{d\sigma}{dE} \right)_{\theta=0^\circ} \approx \frac{4}{\pi} \frac{1}{(\Delta\theta_{1/2})^2} \frac{d\sigma}{dE}, \quad (12)$$

by Serber, for the opaque-nucleus approximation, where $R_A \gg R_d$,

$$\frac{d\sigma}{dE} = \frac{\pi}{4} R_A R_d \frac{B_d E_d}{[(E - \frac{1}{2} E_d)^2 + E_d B_d]^{3/2}}, \quad (13)$$

and

$$\Delta\theta_{1/2} = 1.6(B_d/E_d)^{1/2}, \quad (14)$$

where B_d is the binding energy of the deuteron, 2.225 MeV; R_d is the radius of the deuteron, 2.16×10^{-13} cm; and M_t is the atomic mass of the target nucleus.

By inserting Eqs. (11)–(14) into Eq. (10), the stripping neutron spectrum at 0 deg, $\Phi(E,0)$, was calculated to compare with the measured neutron spectra for thick carbon, copper, and lead targets by normalizing at a certain point. Figure 5 shows the comparison between the calculated spectrum $\Phi_{\text{cal}}(E,0)$ and the neutron spectrum $\Phi_a(E,\theta)$ which might be considered to be the neutrons emitted purely from the deuteron stripping. The $\Phi_a(E,\theta)$ value was estimated by subtracting the continuum spectra, $E \exp[-E/T'(\theta)]$, corresponding to the preequilibrium neutron emission described in the preceding section, from the $\Phi_{\text{exp}}(E,\theta)$ value.

From the figures, the following facts can be found:

(1) The calculated spectrum $\Phi_{\text{cal}}(E,0)$ fits the experimental spectrum $\Phi_a(E,0)$ for carbon well on its high energy side, but it overestimates the number of low energy neutrons. This result is the same situation as those obtained for a neutron spectrum of a thick beryllium target bombarded by deuterons in Refs. 15 and 16. For copper and lead targets, the calculated and experimental spectral shapes are similar together, but the center of the calculated spectrum is significantly shifted to a lower energy than that of the measured spectrum, and this difference becomes larger with an increase in the target atomic mass. This may be because the effect of the Coulomb barrier is evaluated too heavily.

(2) The most probable energy in the measured neutron spectrum at 0 deg is shown in Table III, and that energy for carbon and copper is about $0.4E_0$, which is a well-

TABLE III. Most probable energy and normalization constants of measured and calculated neutron spectra at 0 deg by the deuteron stripping reaction.

Target	Most probable energy (MeV)	$\Phi_a(E,0)/\Phi_{\text{cal}}(E,0)^a$
C	~13	1.23
Cu	~13	0.89
Pb	~10.5	1.36

^aSee text.

established rule for thick target neutron production by deuteron stripping shown in Ref. 15. The calculated spectrum underestimates the most probable energy by about 1 MeV for the carbon target, similarly as in Refs. 15 and 16.

(3) The normalization constants of $\Phi_{\text{cal}}(E,0)$ to $\Phi_a(E,0)$ are also shown in Table III. The value of Φ_{cal}/Φ_a is rather close to 1 for all three targets within about a 30% difference. This means that the Serber model gives rather good absolute values for the deuteron stripping cross section, despite its simplicity.

(4) The neutron yield produced by deuteron stripping decreases and its angular distribution becomes wider with increasing target atomic mass. This means that a nucleon is emitted in the more forward direction from a lighter target since the momentum transfer from the deuteron to a lighter target is greater.

V. CONCLUSION

In this second part of this successive study, we could analyze the measured neutron spectra from thick carbon, copper, and lead targets exposed to 30-MeV proton, 33-MeV deuteron, 65-MeV ^3He , and 65-MeV alpha ions. The measured spectra were divided into two components of evaporation neutrons emitted from a compound nucleus and preequilibrium neutrons from a precompound nucleus, both fitted to a Maxwellian-type spectrum having different nuclear temperatures. For deuteron, ^3He , and alpha ions, a broad bump was clearly seen in the forward neutron spectrum. This bump corresponds to the direct knockout process and the deuteron and ^3He breakup process. The deuteron breakup process was analyzed by the Serber model and showed rather good agreement between calculation and experiment.

The authors wish to thank Prof. Kokame and Ms. Oshikubo for their kind help in using the computer aided graphics and lettering.

¹V. V. Verbinski and W. R. Burrus, Phys. Rev. **177**, 1671 (1969).

²S. M. Grimes, J. D. Anderson, J. C. Davis, and C. Wong, Phys. Rev. C **8**, 1770 (1973).

³E. Gadioli, E. Gadioli Erba, and G. Tagliaferri, Phys. Rev. C **14**, 573 (1976).

⁴M. Blann, R. R. Doering, A. Galonsky, D. M. Patterson, and F. E. Serr, Nucl. Phys. **A257**, 15 (1976).

- ⁵A. Chevarier, N. Chevarier, A. Demeyer, A. Alevra, R. Dumitrescu, I. R. Lukas, M. T. Magda, and M. E. Nistor, Nucl. Phys. A231, 64 (1974).
- ⁶A. Alevra, R. Dumitrescu, I. R. Lukas, M. T. Magda, D. Plostinaru, E. Trutia, N. Chevarier, A. Chevarier, A. Demeyer, and T. M. Duc, Nucl. Phys. A209, 557 (1973).
- ⁷R. A. Cecil, B. D. Anderson, A. R. Baldwin, R. Madey, W. Schimmerling, J. W. Kast, and D. Ortendahl, Phys. Rev. C 24, 2013 (1981).
- ⁸J. W. Wachter, W. R. Burrus, and W. A. Gibson, Phys. Rev. 161, 971 (1967).
- ⁹J. W. Wachter, W. A. Gibson, and W. R. Burrus, Phys. Rev. C 6, 1496 (1972).
- ¹⁰R. Madey and F. M. Waterman, Phys. Rev. C 8, 2412 (1973).
- ¹¹L. R. Veese, R. R. Fullwood, A. A. Robba, and E. R. Shunk, Nucl. Instrum. Methods 117, 509 (1974).
- ¹²R. A. Cecil, B. D. Anderson, A. R. Baldwin, R. Madey, A. Galonsky, P. Miller, L. Young, and F. M. Waterman, Phys. Rev. C 21, 2471 (1980).
- ¹³T. Nakamura, M. Fujii, and K. Shin, Nucl. Sci. Eng. 83, 444 (1983).
- ¹⁴R. Serber, Phys. Rev. 72, 1008 (1947).
- ¹⁵L. S. August, F. H. Attix, G. H. Herling, P. Shapiro, and R. B. Theus, Phys. Med. Biol. 21, 931 (1976).
- ¹⁶R. Madey, F. M. Waterman, and A. R. Baldwin, Phys. Rev. C 14, 801 (1976).
- ¹⁷R. G. Alsmiller, Jr., M. Leimdoerfer, and J. Barish, Oak Ridge National Laboratory Report No. ORNL-4046, 1967.
- ¹⁸H. H. Anderson and J. F. Ziegler, *The Stopping Powers and Ranges in All Elements* (Pergamon, New York, 1977), Vol. 3, p. 16.
- ¹⁹N. Matsuoka, A. Shimizu, K. Hosono, T. Saito, M. Kondo, H. Sakaguchi, Y. Toba, A. Goto, F. Ohtani, and N. Nakanishi, Nucl. Phys. A311, 173 (1978).